



HAL
open science

A TMD-based model for Hadronization off heavy nuclei

Federico Ceccopieri, Raphaël Dupré

► **To cite this version:**

Federico Ceccopieri, Raphaël Dupré. A TMD-based model for Hadronization off heavy nuclei. *Physical Review C*, 2024, 110 (4), pp.045202. 10.1103/PhysRevC.110.045202 . hal-04190254

HAL Id: hal-04190254

<https://hal.science/hal-04190254v1>

Submitted on 31 Oct 2024

HAL is a multi-disciplinary open access archive for the deposit and dissemination of scientific research documents, whether they are published or not. The documents may come from teaching and research institutions in France or abroad, or from public or private research centers.

L'archive ouverte pluridisciplinaire **HAL**, est destinée au dépôt et à la diffusion de documents scientifiques de niveau recherche, publiés ou non, émanant des établissements d'enseignement et de recherche français ou étrangers, des laboratoires publics ou privés.

A TMD-based model for Hadronization off heavy nuclei

F. A. Ceccopieri and R. Dupré*

Université Paris-Saclay, CNRS, IJCLab, 91405, Orsay, France

(Dated: September 20, 2024)

Abstract

Semi-inclusive deep inelastic scattering off nuclei is a unique process to study the parton propagation mechanism and its modification induced by the presence of the nuclear medium. It allows us to probe the medium properties, particularly the cold nuclear matter transport coefficient, which can be directly linked to the nuclear gluon density. We present here a model for hadron production in deep inelastic lepton-nucleus scattering, which takes into account the hadronic transverse momentum of final state particles via transverse-momentum dependent (TMD) parton distributions and fragmentation functions. We implement parton energy loss and hadronic absorption with a geometrical model of the nucleus. The model is compared with the nuclear SIDIS multiplicity ratios and transverse-momentum broadening data from the CLAS, HERMES, and EMC collaborations, aiming for a simultaneous description of these data sets. We obtain a good agreement over the various nuclear targets and the wide kinematical range of those experiments. We best describe the data with a transport coefficient $\hat{q} = 0.3 \text{ GeV}/\text{fm}^2$, and we highlight the importance and the role of correlations in extracting this quantity.

Keywords: first keyword, second keyword, third keyword

*Correspondence email address: raphael.dupre@ijclab.in2p3.fr

I. INTRODUCTION

The fragmentation of quarks into hadrons, *i.e.* hadronization, is a complex dynamical process of QCD. It is extensively studied in the vacuum and can be described by perturbative QCD and non-perturbative fragmentation functions [1]. This process is modified in the presence of a medium, such that studying the modification of the hadron spectra allows the extraction of certain medium properties. Conversely, a medium with known properties can be used for the study of the space-time development of the hadronization process [2]. Such studies require careful consideration of the longitudinal and transverse components of the hadron spectra simultaneously. Here, we will study this problem using a model based on transverse momentum dependent (TMD) parton distribution functions (PDF) and fragmentation functions (FF). Recently, much progress has been made on TMD studies for proton, deuteron, and nuclei [3–5]. We present here a TMD model for hadron production in heavier nuclei and test it against the nuclear hadronization data sets from the EMC [6], HERMES [7–9] and CLAS [10] collaborations.

The present study includes two main nuclear effects: induced energy loss and nuclear absorption. The former is related to elastic collisions of the propagating parton, and the latter to the inelastic collision of the prehadron with nucleons. The interface of those two mechanisms is the production length, L_P , *i.e.* the length necessary for the quark to turn into a color-singlet prehadron. Energy loss and nuclear absorption are complementary, but there is no consensus in the literature on their respective quantitative contributions. The analysis presented in this paper aims at building a model that accommodates both effects and can describe an extensive data set with proper tuning of the production length L_P and the quark transport coefficient, \hat{q} . The latter is the key parameter of induced energy loss calculations, defined as the amount of transverse momentum the parton gains per unit of length of traversed material. The hadron production in semi-inclusive deep-inelastic scattering (SIDIS) off nuclei is the best process for extracting those quantities.

Several groups have performed similar work in the past [11–14], often with a focus on energy loss [15–22]. Monte-Carlo event simulation is also sometimes used to approach the problem in a fully consistent way [23, 24] with the advantage of naturally including correlations. We aim to extend these previous works by using a TMD framework to describe the longitudinal and transverse components, as well as their correlations.

II. TMD CROSS SECTIONS

We consider the process

$$\ell(l) + N(P) \rightarrow \ell(l') + h(P_h) + X, \quad (1)$$

where ℓ denotes the beam lepton, N the nucleon target, h the produced hadron and X the remainder of the hadronic final state. Particles four-momenta are given in parentheses. As customary, we define the photon momentum to be $q = l - l'$, and we introduce the invariants $Q^2 = -q^2$, $\nu = p \cdot q/M$, $x_B = Q^2/2P \cdot q$, $y = P \cdot q/P \cdot l$, $W^2 = (P + q)^2$, and $z = P \cdot P_h/P \cdot q$. We define $P_{h\perp}$ to be the transverse components of hadron momentum P_h with respect to the virtual photon momentum, defined in the target rest frame and ϕ_h the angle between the leptonic and the hadronic planes following the Trento convention [25]. Throughout this paper, we work in the one-photon exchange approximation and neglect the lepton mass. We retain in the calculation, when necessary, the nucleon mass M and the hadron h mass, M_h . The semi-inclusive lepton-hadron cross-section, summed over the helicities of the incoming lepton, can be written as [26]

$$\frac{d^5\sigma}{dx_B dy dz dP_{h\perp}^2 d\phi_h} = \frac{\pi\alpha^2}{Q^2 x_B y} \left\{ [1 + (1 - y)^2] F_{UU,T} + 2(2 - y) \sqrt{1 - y} F_{UU,T}^{\cos\phi_h} \cos\phi_h + 2(1 - y) F_{UU,T}^{\cos(2\phi_h)} \cos(2\phi_h) \right\}, \quad (2)$$

where the structure functions on the r.h.s. depends on x_B , Q^2 , z and $P_{h\perp}^2$. The first and second subscripts of the above structure functions indicate the respective polarization of the beam and the target, whereas the third subscript specifies the polarization of the virtual photon. As all our analysis is performed at the lowest order in the strong coupling, the contributions corresponding to photon longitudinal polarization are absent at this order of accuracy. The structure function $F_{UU,T}$ can be expressed as a convolution over partonic transverse momenta as

$$F_{UU,T} = x_B \sum_q e_q^2 \int d^2\mathbf{p}_\perp d^2\mathbf{k}_\perp \delta^{(2)}(\mathbf{p}_\perp + z\mathbf{k}_\perp - \mathbf{P}_{h\perp}) f_{q/P}(x_B, Q^2, \mathbf{k}_\perp) D_{h/q}(z, Q^2, \mathbf{p}_\perp), \quad (3)$$

where $f_{q/P}(x_B, Q^2, \mathbf{k}_\perp)$ and $D_{h/q}(z, Q^2, \mathbf{p}_\perp)$ represent the TMD unpolarised parton distribution in the proton and TMD unpolarised fragmentation functions, respectively. Here \mathbf{k}_\perp represents the transverse momentum of the initial state parton with respect to the virtual photon direction and \mathbf{p}_\perp the transverse momentum of the detected hadron relative to the

fragmenting parton. Both distributions are evaluated at the virtuality Q^2 of the photon. The delta function results from transverse momentum conservation. The summation runs over quarks and antiquarks at this order. In the following, we will turn these expressions into a form suitable for phenomenological applications. Convolution integrals in Eq. (3) can be analytically performed under the hypothesis that the transverse momentum and the light-cone fraction dependencies of TMD densities could be factorized by assuming a Gaussian shape of the transverse part; such an assumption is known to be good at low transverse momentum. Therefore, we use for the TMD PDFs and FFs, the following ansatz:

$$f_{q/P}(x_B, Q^2, \mathbf{k}_\perp) = f_{q/P}(x_B, Q^2) \frac{1}{\pi \langle k_\perp^2 \rangle} e^{-k_\perp^2 / \langle k_\perp^2 \rangle} \quad (4)$$

and

$$D_{h/q}(z, Q^2, \mathbf{p}_\perp) = D_{h/q}(z, Q^2) \frac{1}{\pi \langle p_\perp^2 \rangle} e^{-p_\perp^2 / \langle p_\perp^2 \rangle}. \quad (5)$$

Within this approximation, TMD PDFs and FFs are normalized to give the corresponding collinear distributions upon integration over transverse momentum. In the present analysis, we include the evolution of the above collinear functions, as indicated by the explicit Q^2 dependence in the relevant functions, but we neglect the full TMD evolution, which would unnecessarily weight down the formalism and would require additional modelization in the nuclear case [5]. This simplified approach also allows us to include the transverse momentum broadening when considering SIDIS on nuclear targets in a relatively economical way, which is crucial to us given the time-consuming cross sections evaluation of that specific case.

In such approximations, the structure function in Eq. (3) can be eventually rewritten as:

$$F_{UU,T} = x_B \sum_q e_q^2 f_{q/P}(x_B, Q^2) D_{h/q}(z, Q^2) \frac{e^{-P_{hT}^2 / \langle P_{hT}^2 \rangle}}{\pi \langle P_{hT}^2 \rangle}. \quad (6)$$

Its structure is dictated by the convolution over transverse momenta from Eq. (3) and the Gaussian assumption on the transverse part in Eq. (4) and Eq. (5). The full width $\langle P_{hT}^2 \rangle$ being the average hadronic transverse momentum is then of the form:

$$\langle P_{hT}^2 \rangle = \langle p_\perp^2 \rangle + z^2 \langle k_\perp^2 \rangle. \quad (7)$$

In general, we do not expect the shape of the hadronic width $\langle P_{hT}^2 \rangle$ to have a significant impact on our nuclear observables, which by construction isolate nuclear effects. However, some dependence may arise due to correlations in the integration of the model over the

experimental bins, which will likely introduce some sensitivity on the z -shape of $\langle P_{hT}^2 \rangle$. For that reason, we made a dedicated extraction of $\langle P_{hT}^2 \rangle$ whose details are collected in Appendix A.

Finally, realistic results are obtained only after the proper implementation of the kinematic cuts used in the data set we try to reproduce. In particular, the contribution of target fragmentation is not accounted for in our formalism. Therefore, we apply a cut on Feynman x , with $x_F = 2h_z^*/W$, h_z^* being the hadron third component defined in the γ^*P center-of-mass frame, whenever specified by the kinematical selection of a given data set. Next, we consider the cut on the invariant mass of the system X (M_X), where the latter represents the hadronic final state but with the measured final state hadron h excluded. In all our calculations, we enforce the condition $M_X > M$, which induces a sizeable decrease of the $P_{h\perp}$ -width at large z and low ν .

III. NUCLEAR EFFECTS

The two main observables used by the experiments are the multiplicity ratios

$$R_h^A(\nu, Q^2, z, P_{hT}^2) = \frac{N_h^A(\nu, Q^2, z, P_{hT}^2)/N_e^A(\nu, Q^2)}{N_h^D(\nu, Q^2, z, P_{hT}^2)/N_e^D(\nu, Q^2)}, \quad (8)$$

and the transverse momentum broadening

$$\Delta\langle P_{hT}^2 \rangle = \langle P_{hT}^2 \rangle_A - \langle P_{hT}^2 \rangle_D, \quad (9)$$

where A stands for the atomic mass number, N_e and N_h the number of inclusive and semi-inclusive events, respectively, and the observables being both normalized to deuterium, D . In the present analysis, we will not provide an extensive comparison of all particle species, but we will compare our model with multidimensional data sets whenever possible to account for possible correlations in the data. For this reason, we focus on positively charged pions: they are abundantly produced, such that precise fragmentation functions are available. In addition, they are nearly massless, which avoids theoretical issues due to hadron mass corrections.

A. Production length and nuclear medium density

We implement the nuclear effects under the hypothesis that energy loss occurs before absorption. Thus, we need to know the length of the total traversed material and the production length L_P , where parton energy loss ends and absorption starts. To go further and account for the density profile of the nucleus, we need to define effective lengths. To do so, we assume that the incident photon scatters on a parton belonging to a nucleon at position x_i, \vec{b}_i , with the origin fixed to the nuclear center. The scattered parton then moves along the positive x direction. We describe the nuclear matter distribution with a Wood Saxon distribution, $\rho(x, \vec{b}_i)$, normalized to A . With this in mind, we adopt the following definition of total path length traversed in nuclear matter:

$$L_T^*(x_i, \vec{b}_i) = \frac{1}{\rho(0, 0)} \int_{x_i}^{\infty} dx \rho(x, \vec{b}_i). \quad (10)$$

The production length, *i.e.* the length traveled by the colored parton before forming a pre-hadron, is parametrized with the following form:

$$L_P(z, \nu) = N z^\lambda (1 - z)^\beta \left(\frac{\nu}{\text{GeV}} \right)^\gamma. \quad (11)$$

Generally, one expects $\lambda \simeq \beta \simeq \gamma \simeq 1$ to reflect the Lorentz boost and fragmentation constraints on the parton lifetime. These settings have not provided a satisfactory description of data in the past and have been modified or complemented in various ways in the literature [2, 11, 12, 15]. Here, we introduce these parameters, but we adjust them to better describe the data. To limit the number of parameters, we do not explore the interesting possibility that L_P might depend on other variables, such as P_{hT}^2 or Q^2 [11, 27]. Similarly to the total path length L_T^* , we define an effective production length

$$L_P^*(z, \nu; x_i, \vec{b}_i) = \frac{1}{\rho(0, 0)} \int_{x_i}^{x_i + L_P(z, \nu)} dx \rho(x, \vec{b}_i), \quad (12)$$

which, at variance with Eq. (10), takes into account the finite production length L_p in the upper integration limit.

B. Partonic energy loss

When partons traverse a QCD medium such as the nucleus, we expect them to emit gluons and lose some of their energy. Several groups have tackled the problem of calculating

this energy loss with a rather large spread of results [28]. We chose to use the calculation by Arleo [29], based on the BDMPS calculations [30, 31]. In this framework, the energy loss ϵ depends on the transport coefficient and the length of the medium through the characteristic gluon energy

$$w_c = \frac{1}{2} \hat{q} L_P^{*2}. \quad (13)$$

The energy loss probability distribution $W(\epsilon)$ by Arleo includes also the dependence on the outgoing parton energy, which we take to be ν . It is expressed as follows:

$$\overline{W}(\bar{\epsilon}, \bar{\nu}) = \frac{1}{\sqrt{2\pi} \sigma(\bar{\nu}) \bar{\epsilon}} \exp \left[-\frac{(\log \bar{\epsilon} - \mu(\bar{\nu}))^2}{2 \sigma(\bar{\nu})^2} \right], \quad (14)$$

where barred variables are normalized to ω_c , the functions μ and σ are empirical [29] and its normalized version is defined by $\overline{W}(\bar{\epsilon} = \epsilon/\omega_c) = \omega_c W(\epsilon)$. We model nuclear-modified FFs according to the kinematic rescaling proposed by Wang, Huang and Sarcevic [32], which amounts to shift the argument of the collinear FFs:

$$z_* = \frac{z}{1 - \epsilon/\nu}. \quad (15)$$

The implementation of such a rescaling allows us to obtain the nuclear-modified TMD FFs:

$$z D_{h/q}^A(z, \nu, Q^2, p_\perp) = \int_0^{(1-z)\nu} d\epsilon W(\epsilon, \nu, \hat{q}, L_P^*) z_* D_{h/q}(z_*, Q^2, p_\perp), \quad (16)$$

which generalizes the collinear variables rescaling proposed in Ref. [32] to transverse ones. For clarity, we have omitted its dependence via L_P^* on the position x_i, \vec{b}_i of the nucleon in the nucleus on which the incident photon scatters. Moreover, we use the connection proposed by BDMPS to link the energy loss ϵ to $\langle q_\perp^2 \rangle$, the average transverse momentum acquired by the parton traversing the medium [33, 34]:

$$-\frac{dE}{dx} = \frac{\alpha_s N_C}{4} \langle q_\perp^2 \rangle, \quad (17)$$

with E the energy of the gluon emitter, x is the distance traversed by the parton, N_C the number of colors, α_s the strong coupling constant. From this, we can link the transverse momentum broadening to the parton energy loss:

$$\langle q_\perp^2 \rangle = \frac{4\epsilon}{\alpha_s N_C L_P^*}, \quad (18)$$

We assume that this source of transverse momentum is distributed according to a Gaussian of width $\langle q_\perp^2 \rangle$. Since it is acquired during the in-medium fragmentation process, its width

is scaled by a factor z_*^2 . As a result, the overall nuclear-modified fragmentation width is given by $\langle p_\perp^2 \rangle_A = \langle p_\perp^2 \rangle(z_*) + z_*^2 \langle q_\perp^2 \rangle$. Within these approximations, the nuclear-modified fragmentation function in Eq. (16) can be written as

$$D_{h/q}^A(z, \nu, Q^2, p_\perp) = \int_0^{(1-z)\nu} d\epsilon \frac{W(\epsilon, \nu, \hat{q}, L_P^*)}{1 - \epsilon/\nu} D_{h/q}(z_*, Q^2) \frac{e^{-p_\perp^2 / \langle p_\perp^2 \rangle_A}}{\pi \langle p_\perp^2 \rangle_A}. \quad (19)$$

C. Absorption

After the production length, a prehadron starts to form and might interact with the medium, thus not giving rise to a measured hadron in the final state. To simulate this, we use an attenuation factor of the form:

$$n_{att}(z, \nu; x_i, b_i) = 1 - \left[\frac{L_T^* - L_P^*}{L_{typical}} \right]^d, \quad (20)$$

with $L_{typical}$ and d free parameters. This parametrization is constructed such as to introduce a correlation between the length traversed by the prehadron in the medium, $L_T^* - L_P^*$, and the absorption process. Given the definition in Eq. (10) and Eq. (12), the latter quantity is greater than zero by construction and, at any fixed value of L_T^* , the attenuation is maximal when $L_P^* \rightarrow 0$. The attenuation factor n_{att} implicitly depends on z and ν through the dependence of L_P on those variables. We further assume that it is quark-flavor independent and apply it as a multiplicative factor in defining nuclear FFs in Eq. (16).

We do not attribute transverse momentum in association with the pre-hadron interaction as the elastic process contributes very little compared to inelastic processes [16]. Thus, we consider here that the pre-hadrons are absorbed in the nucleus, giving rise to fragments in the target fragmentation region outside our model's domain.

D. Fermi motion

Among the initial state effects we need to consider is the Fermi motion of the nucleons in the nuclear targets. We use the parametrizations of 3-momentum distributions, $n_A(\vec{P})$ presented in Ref. [35], with \vec{P} the nucleon three-momentum in the nucleus. We neglect the effect of Fermi motion in the longitudinal direction due to its small size relative to the typical energies involved in the experiments we aim to describe. As we only consider the transverse

contribution, we define the average transverse Fermi motion as

$$\langle P_T^2 \rangle_A = \frac{\int d^3\vec{P} P_T^2 n_A(\vec{P})}{\int d^3\vec{P} n_A(\vec{P})}, \quad (21)$$

where adopting spherical coordinates, the transverse momentum is defined with respect to the z -axis, corresponding to the incoming photon direction. Projecting out transverse components, the integral can be written as

$$\langle P_T^2 \rangle_A = \frac{2}{3} \int_0^\infty P^4 dP n_A(P). \quad (22)$$

The calculation returns an average transverse Fermi motion of around 0.011 GeV^2 for deuterium which rises fast to 0.036 GeV^2 for carbon, and then flattens out for heavier nuclei and ends around 0.044 GeV^2 for a lead nucleus.

This source of initial state transverse momentum, assuming it is distributed as a Gaussian with widths provided by the calculation, adds to the initial state partonic transverse momentum. Therefore, as dictated by transverse kinematics in eq. (7), the corresponding widths will sum up and will be weighted by a factor z^2 .

E. Nuclear structure functions

Putting together all the elements discussed above, the unpolarized nuclear structure function reads

$$F_{UU,T}^A = x_B \sum_q e_q^2 f_{q/A}(x_B, Q^2) \int dx_i \int d^2\vec{b}_i \frac{\rho(x_i, b_i)}{A} \int_0^{(1-z)\nu} d\epsilon \frac{W(\epsilon, \nu, \hat{q}, L_P^*)}{1 - \epsilon/\nu} n_{att}(z, \nu; x_i, b_i) D_{h/q}(z_*, Q^2) \frac{e^{-P_{hT}^2 / \langle P_{hT}^2 \rangle(z_*)}}{\pi \langle P_{hT}^2 \rangle(z_*)}, \quad (23)$$

where $f_{q/A}$ are the nuclear PDFs for which we adopt the set **nCTEQ15** [36], and $D_{h/q}$ are the vacuum parton-to-pion fragmentation functions for which we adopt the **DEHSS** set [37]. In general, for the observable studied in the present paper, the predictions are rather independent of the choices of the specific sets of PDFs and FFs.

We assume that all sources of transverse momentum broadening have a Gaussian distribution such that their convolution gives an overall Gaussian with a width

$$\langle P_{hT}^2 \rangle_A = \langle p_\perp^2 \rangle(z_*) + z^2[\langle k_\perp^2 \rangle + \langle P_T^2 \rangle_A] + z_*^2 \langle q_\perp^2 \rangle. \quad (24)$$

The first term is the width of the fragmentation function but evaluated, according to Eq. (16), at z_*^2 . The terms weighted by z^2 are for the initial state parton momenta intrinsic in the nucleon and the nuclear Fermi motion. The last term accounts for the nuclear broadening due to parton energy loss and is weighted by z_*^2 .

The observables introduced in Eq. (8) and Eq.(9) are both normalized to the deuterium. Such a normalization point is commonly used since deuterium does not show any nuclear effect, allowing hadronization to be described in terms of vacuum fragmentation functions. However, the model discussed so far, designed to describe hadronization off heavy nuclei, shows sizeable nuclear effects when extrapolated to very light nuclei like deuterium. Therefore, to ensure a proper subtraction of spurious effects and a consequent correct normalization of the observables, we normalize the predictions to our extrapolated version of deuterium.

IV. RESULTS

The large number of convolutions makes theory predictions time-consuming and not suitable for a fit. To overcome this problem, we first studied the model's behavior in parameter space and then fixed the latter via a tuning procedure that allows us to fairly describe all data sets at once.

A. Energy loss only parameterization

Among the two mechanisms we consider, the partonic energy loss has been extensively studied in the literature and has a solid theoretical background. Therefore, in the first attempt, we tried to describe the data with that mechanism alone responsible for both the depletion of hadron yields and the broadening of the transverse momentum.

Within this picture, the parton will radiate all the way out of the nucleus, *i.e.* $L_P \rightarrow \infty$, maximizing the amount of radiated energy, the hadronization will occur outside the nucleus, and no absorption will take place, *i.e.* $n_{att} = 1$. Under this approximation, we present in the top panels of Fig. (1) the comparison of the HERMES multiplicity ratios as a function of z and P_{hT}^2 with our default value $\hat{q} = 0.3 \text{ GeV}/\text{fm}^2$. The multiplicity ratios show a clear deficit in normalization (leftmost panels) while the transverse momentum broadening, $\Delta\langle P_{hT}^2 \rangle$, is

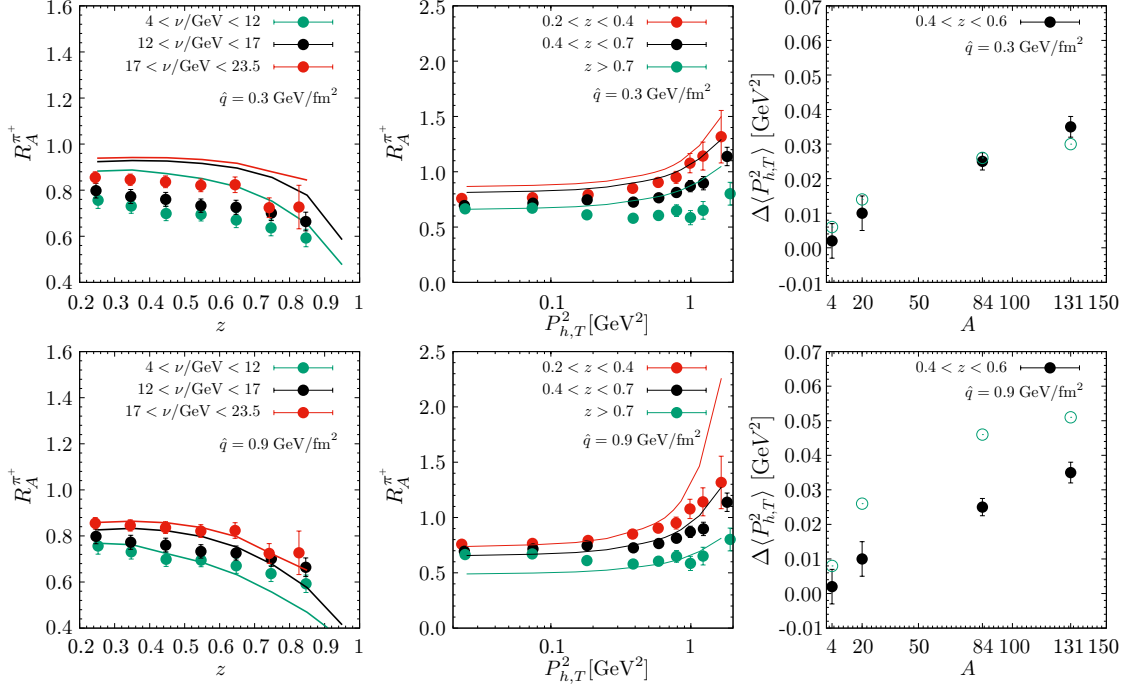


Figure 1: Predictions within an “energy loss alone” model, *i.e.* $L_P \rightarrow \infty$, with $\hat{q} = 0.3 \text{ GeV/fm}^2$ in top panels and $\hat{q} = 0.9 \text{ GeV/fm}^2$ in bottom ones. We present the π^+ -multiplicity ratios on a Krypton target as a function of z in the leftmost column and as a function of P_{hT}^2 in the middle one. In the rightmost column, we present the $\Delta\langle P_{hT}^2 \rangle$ -broadening as a function of A . Data from the HERMES collaboration [8].

fairly reproduced (rightmost panel). The normalization issue of the former can be alleviated by using a larger value of $\hat{q} \approx 0.9 \text{ GeV/fm}^2$, as shown in the bottom left panels of Fig. (1). However, such a large \hat{q} entering in Eq. 17, leads to an abnormally large $\Delta\langle P_{hT}^2 \rangle$, by far greater than the one seen in the data (bottom right panel). We conclude that with an energy loss model alone, we can not describe those observables simultaneously with a single value of \hat{q} . However, such an issue can be overcome by assuming that another mechanism is at work to reduce the yields, *i.e.* absorption. The attenuation is produced by inelastic interactions of the so-called prehadrons, a colorless state yet to become real hadron, with the medium, possibly creating secondary particles with lower energies. Under the hypothesis that elastic prehadron-nucleon cross sections are small, this mechanism generates neither broadening nor energy loss.

Production length			
N	λ	β	γ
4.0 fm	0.0	0.25	0.3
Transport coefficient		Nuclear absorption	
\hat{q}	α_s	$L_{typical}$	d
0.3 GeV/fm ²	0.5	2 fm	0.5

Table I: Numerical values of the parameters controlling the production length, the transport coefficient and nuclear absorption.

B. Full model parametrization

We include the *ad hoc* absorption from Eq. 20 for which we need to find suitable parameters. Our aim is not to make the best possible description of the data in all corners like in a fit. To adjust our parameters, we concentrate on kinematics which are the safest in terms of TMD factorization [38] ($0.3 < z < 0.8$), parton energy loss applicability ($\nu > 10$), and the Gaussian TMD model ($P_{h\perp}^2 < 0.5 \text{ GeV}^2$). We will check later whether our model can be extrapolated out of this kinematic region, so we concentrate here on a subset of the HERMES data [8, 9] to tune our parameters.

We show in Fig. 2 and Fig. 3 a selection of data according to the criteria listed above together with the model with adjusted parameters summarized in Tab. I. The overall agreement is satisfactory, but a few preliminary comments can be made immediately about the parameters obtained. We notice that the exponent parameters for the production length (λ , β and γ) are small compared to previous modelisations [2]. In particular, with $\lambda = 0$ and $\beta = 0.25$, we significantly suppress the z dependence of L_P to describe the data adequately. This is needed so as not to over-suppress the hadron yield at both z extremes. We show in Tab. II the typical production lengths obtained with this set of parameters for the CLAS, HERMES, and EMC data. We observe that these results are consistent with previous work [2].

We obtain a transport coefficient value for cold nuclear matter, $\hat{q} = 0.3 \text{ GeV/fm}^2$, which is larger than some of the most recent extractions [21, 22]. However, these previous works

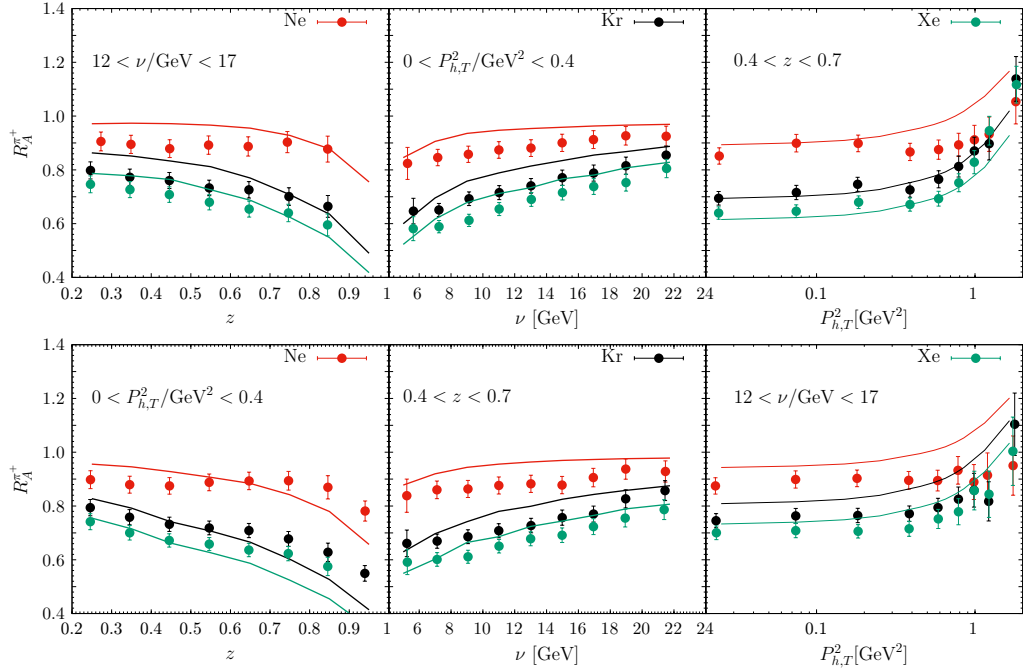


Figure 2: Multiplicity ratio for π^+ on different nuclear targets as a function of various kinematical variables in selected ranges compared to our model with parameters as in Tab. [I]. Data from the HERMES collaboration [8].

	E_{beam}	$\langle \nu \rangle$	$\langle z \rangle$	L_P
	[GeV]	[GeV]		[fm]
CLAS	5	3	0.5	4.7
HERMES	23.5	10	0.5	6.7
EMC	280	100	0.35	14.3

Table II: Values of L_P in the average kinematics of different experiments whose data are considered in this paper.

neglect the correlation between longitudinal and transverse components. We attribute our different result to a survivor bias: because the measured transverse momentum broadening is obtained only through the detected hadrons, it is thus indirectly affected by absorption. In the HERMES data, the hadron yield is reduced by 20-30% in Krypton, whatever model is used, it is clear that the suppressed part of the spectrum will be strongly correlated to the

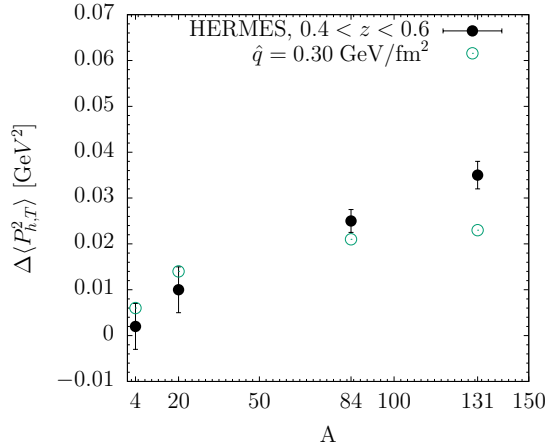


Figure 3: The π^+ transverse momentum broadening in the range $0.4 < z < 0.6$ as a function of A compared to our model with parameters as in Tab. [I]. Data from the HERMES collaboration [8].

length of nuclear material traversed. So effectively, the transverse momentum observables select hadrons that have interacted less with the nuclear medium. Thus, it creates a correlation between absorption and energy loss that reduces the measured transverse momentum broadening and motivates the use of a larger \hat{q} . This effect can already be observed in our first test with energy loss only in Fig. 1. There, it is clear that despite a factor 3 in \hat{q} between the two scenarios explored, the transverse momentum broadening increases by less than a factor 2 for krypton. Together, our results indicate that this effect is large no matter what the source of the hadron yield quenching is, and thus it needs to be accounted for in the description of the transverse-momentum dependent observables.

With the hadron absorption parameters, we can notice that the coefficient d indicates the dependence on the path length. Our best value, $d = 0.5$, indicates that the pre-hadron absorption is reducing as it propagates. Such behavior is possible through a filtering effect where compact prehadrons survive longer, and thus, the absorption effect drops. However, this is in direct contradiction with the results of previous studies [11, 14, 23], which would favor $d = 1$ or 2. The differences between the results presented in these studies and our approach are numerous, but the key difference is likely linked to the way L_P is parameterized. Finally, on the question of hadron absorption, we note that the value of $L_{typical}$ is rather small and hints at a rather large prehadron-nucleon cross-section.

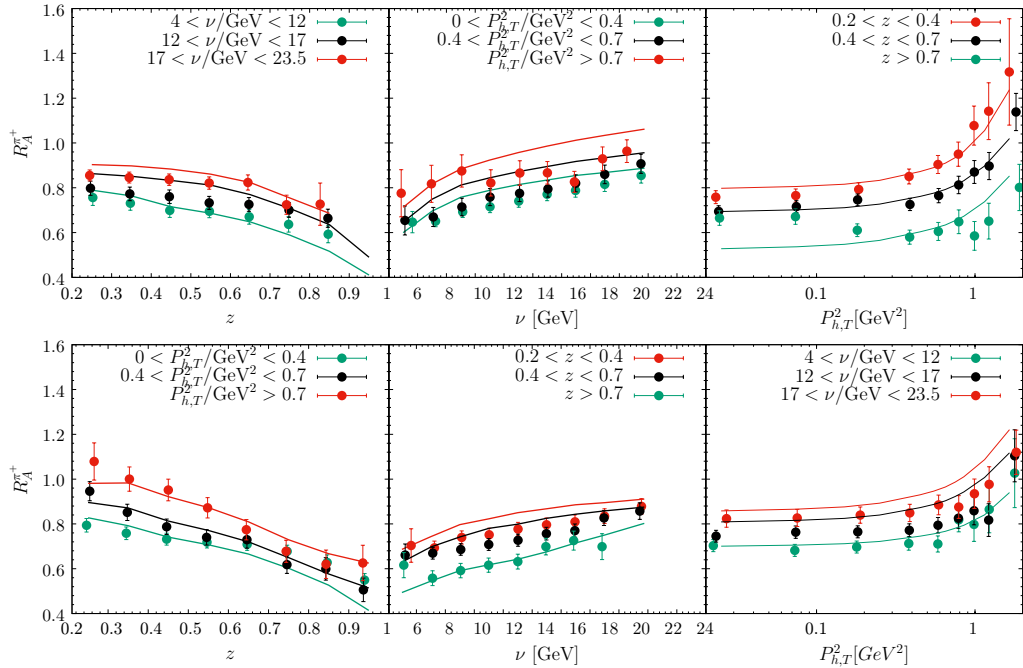


Figure 4: Multiplicity ratio for π^+ on a Krypton target as a function of kinematic variables compared to our model with parameters as in Tab. [I]. Data from the HERMES collaboration [8].

C. Comparison to HERMES data

Going into more details on Fig. 3, we observe that the A dependence of Δp_T^2 is not completely satisfactory, as the model overshoots the light nuclei and undershoots heavier nuclei. This problem is a common feature of numerous descriptions of this observable in the literature [16, 20–22]. The best description we obtain of this observable is in Fig. 1, where production length is set to infinity and absorption is thus completely deactivated. It appears impossible to resolve this issue with existing model frameworks because reducing the production length to increase the absorption contribution further degrades the description of this observable. We conclude that all the models (ours included) are still missing an element contributing to the shape of the transverse momentum broadening as a function of the atomic number A . We compare our model to more HERMES multiplicity ratio data in Fig. 4, and note that all displayed dependencies are pretty well reproduced. Some of the high z behaviors are missed. However, as discussed above, this is a phase space where TMDs do not dominate the cross-section. Thus, we do not expect our model to describe this phase properly. To further analyze the behavior of the model, we compare

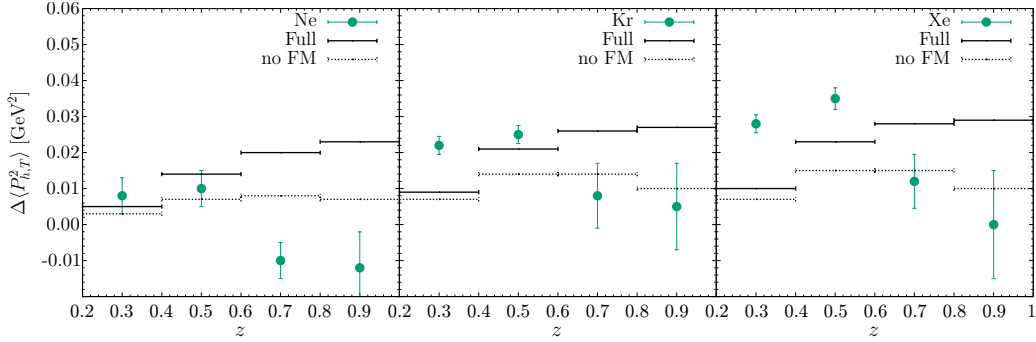


Figure 5: Transverse momentum broadening on various heavy nuclei as a function of z compared to HERMES data of Ref. [8]. Our model, with parameters as in Tab. [I], is shown with (solid lines) and without (dotted) Fermi motion contribution.

predictions for transverse momentum broadening on different targets as a function of z in Fig. (5). We observe that the transverse momentum broadening shape as a function of z appears to be largely off for all nuclear targets. At low z , this is to be expected as target fragmentation might contribute, but at large z the discrepancy is more puzzling. Given the structure of Eq. (24), the rising pattern of $\Delta\langle P_{hT}^2 \rangle$ against z is however expected. Of the previously cited literature, only Domdey et al. [16] shows the same observable, reporting a similar discrepancy. Furthermore, we show our model with and without Fermi motion in the same figure. We observe that the latter is the main contribution at large z . The absence of such a basic effect in the data is surprising. We suspect correlated errors in the data to be at the origin of this behavior, as all nuclei are normalized to the same deuterium data. Otherwise, that would indicate that factorization is largely broken in this kinematical region. To reduce the Fermi motion contribution to the broadening effect, it is also possible to normalize the observable to heavier nuclei like helium, carbon, or neon, for which Fermi motion contribution is much larger than deuterium.

D. Comparison to CLAS data

A critical test for the model and its various components is to check whether it can describe data at different collision energies. To that purpose, we compare our model predictions, with unchanged parameters, to the multiplicity ratio for positively-charged pions measured by the CLAS Collaboration [10]. The lower energy of the beam ($E_e = 5.014$ GeV) implies a much

lower range of lepton energy transfer variable ν as compared to the HERMES case, and the applicability of the TMD factorization and framework at such low energy on nuclei is questionable. Nevertheless, we found, in general, a satisfactory agreement between our model and the data, but some features are worthwhile to discuss.

In Fig. (6) we present the multi-dimensional multiplicity ratios as a function of z for three ν ranges and three target nuclei. For clarity, we did not show the different Q^2 bins in this figure since the dependence on this variable is very weak, a feature also reproduced by our model. The simulations reproduces very well the z -shapes across different values of ν and A while it slightly overshoots the multiplicity ratio for the light target (carbon) and slightly undershoots the one on the heavier target (lead). The data does not show a dependence on ν in contrast with HERMES results, a feature reproduced by our model in this energy range. In the same figure, we present our calculation with absorption switched off, *i.e.* setting $n_{att} = 1$ in Eq. (20), in dotted lines. Comparing the two sets, one may observe that the impact of absorption for this data set is maximal and increasing in going from light to heavier nuclei, a direct consequence of the correlation introduced by the absorption mechanism in Eq. (20).

In Fig. (7), we present the multiplicity ratios as a function of the hadronic P_{hT} in slices of z for different nuclear targets. Setting aside the visible normalization issue in some z bins outlined above, we notice two things. First, the slope of the multiplicity ratios as a function of P_{hT} is reduced as we go to higher z , which our model describes correctly at small P_{hT} . Second, we are significantly undershooting the highest points in P_{hT} . This could be a sign that the model generates an amount of broadening smaller than the one in the data, particularly with this discrepancy getting more pronounced going from light to heavy nuclei. However, it could also be the effect of reaching the end of the phase space in missing mass or due to the non-Gaussian nature at such high P_{hT} . In the absence of transverse momentum broadening results from CLAS, it is difficult to draw definite conclusions on this point.

E. Comparison to EMC data

We finally compare our model to the multiplicity ratios data from the EMC collaboration on a copper target [6]. The collected data refer to multiplicity ratios for the sum of charged hadrons, which we approximate as the sum of charged pions since the latter largely dominates

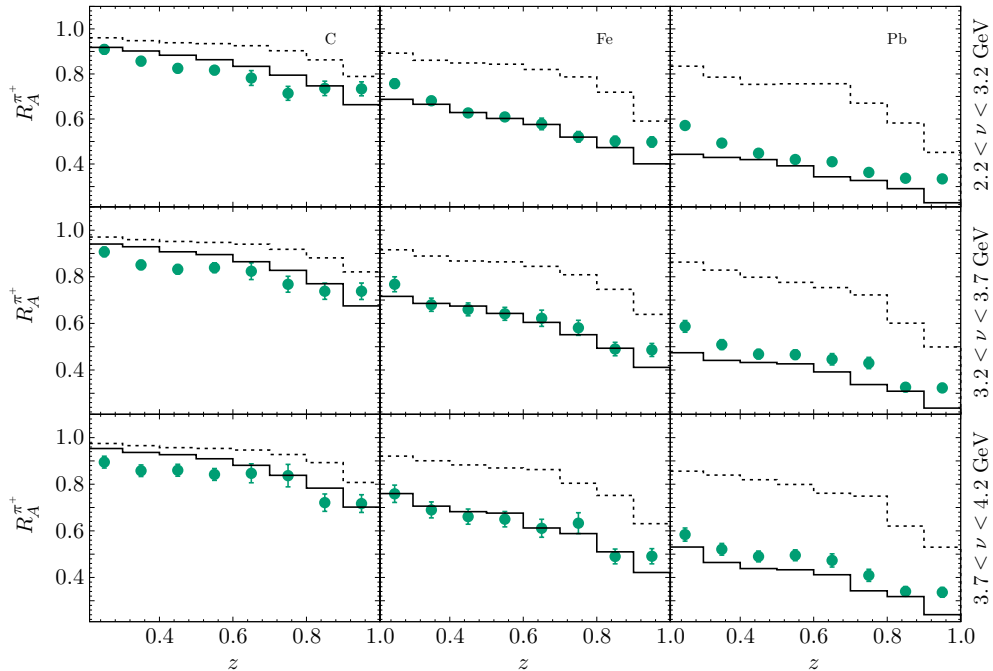


Figure 6: π^+ multiplicity ratios as a function of z for three different nuclear targets integrated in bins of ν and in $1.3 < Q^2 < 1.8 \text{ GeV}^2$. Model predictions are shown with default values (solid lines) and with absorption switched off (dotted), *i.e.* setting $n_{att} = 1$ in Eq. (20). Data from CLAS Collaboration [10].

the hadronic yields. This data set is particularly handy since it allows us to test our model in the transition region from intermediate values of $\nu \approx 20 \text{ GeV}$ up to the asymptotic limit, where nuclear effects vanish.

In Fig. (8), we present our model compared to data. The overall description is very good, particularly the shape of multiplicity ratios as a function of z and ν . We also present the calculation with absorption switched off (dotted lines): the comparison with the full model shows that, given the larger energy transfer, absorption has a much weaker impact on this data set. Nevertheless, absorption still gives a sizeable correction at the lower ν and is necessary to match the normalization and shape observed in the data. We conclude that the energy extrapolation is modeled correctly and reproduces the vanishing of nuclear effects at high energies.

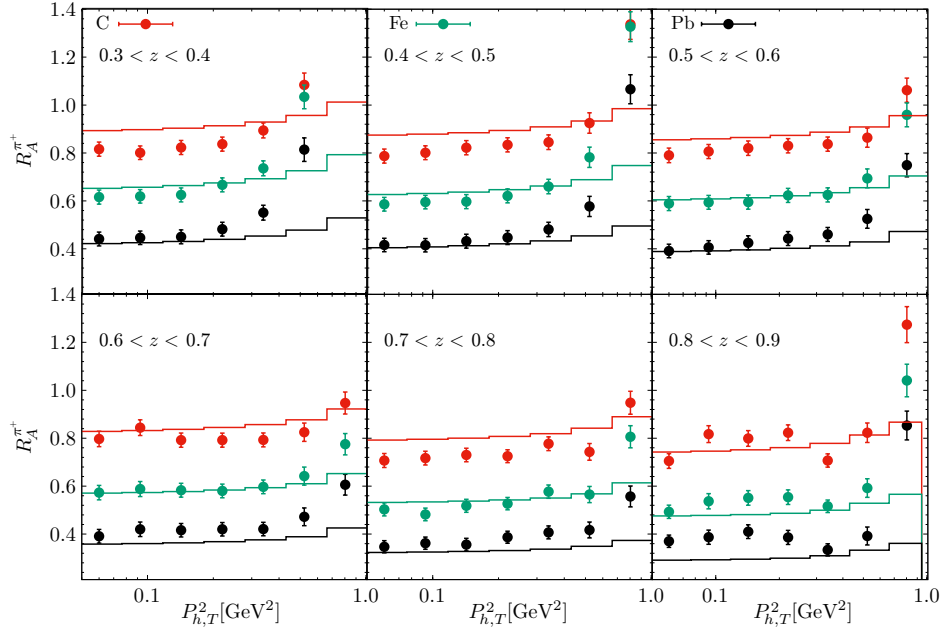


Figure 7: Multiplicity ratios of π^+ as a function of $P_{h,T}^2$ in various z bins for three different nuclear targets. Data from CLAS Collaboration [10].

V. CONCLUSIONS

We applied a TMD-based model to describe the nuclear SIDIS data of the CLAS, HERMES, and EMC collaborations, with the aim of a simultaneous description of multiplicity ratios and transverse momentum broadening. We found that using a model with parton energy loss alone leads to inconsistencies in the combined description of those observables, which can be achieved by adding a pre-hadron absorption mechanism instead. After tuning the model parameters, we found a satisfactory agreement with all the data sets considered. We best describe the data with a cold nuclear matter transport coefficient value $\hat{q} = 0.3 \text{ GeV}/\text{fm}^2$, but this value is strongly correlated with the parametrization of both the absorption mechanism and the production length L_P .

We find strong correlations between the observables and, in particular, an important effect of survivor bias on the transverse momentum broadening measurement. This demonstrates the importance of simultaneously describing both observables to extract the transport coefficient, and more generally, to study the transverse effects in nuclei and understand hadronization off nuclei in SIDIS. The model describes the data on a very wide range of

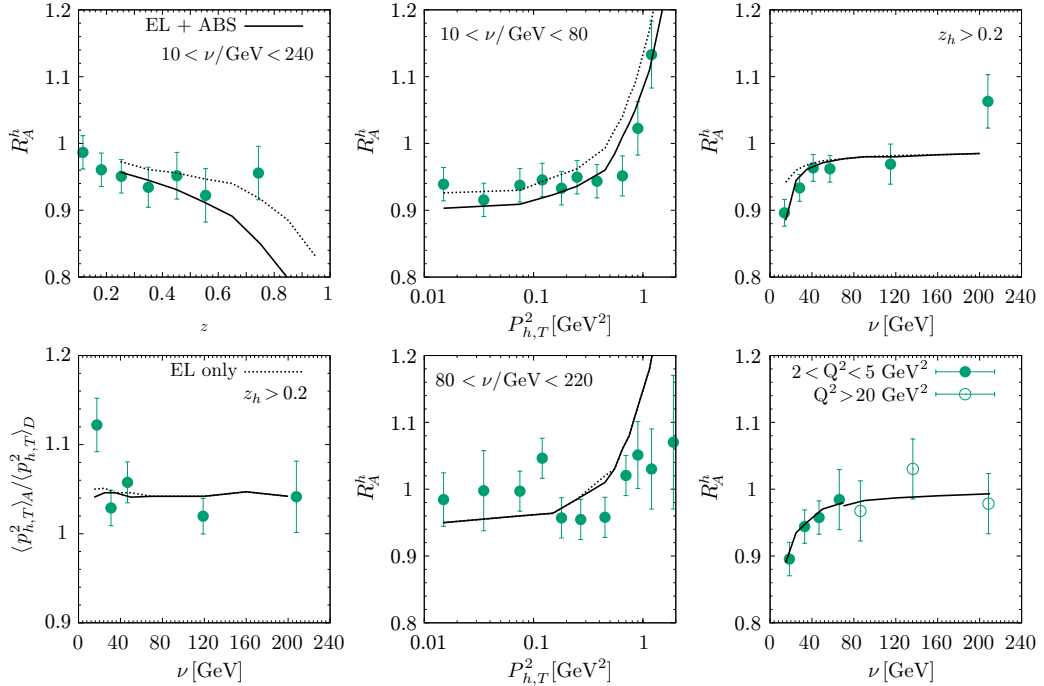


Figure 8: Charged hadrons multiplicity ratios on copper as a function of kinematic variables compared to data from the European Muon Collaboration [6]. Solid lines are for the full model with energy loss plus absorption, while dashed ones are for the model with absorption switched off by setting $n_{att} = 1$. The bottom left panel shows the ratio of hadronic average transverse momentum on the nucleus over that on the deuterium.

energies from $\nu = 2$ GeV to $\nu = 200$ GeV. We find that at low lepton energy transfer, hadron absorption is responsible for the majority of the depletion observed in multiplicity ratios, while at higher lepton energy transfer, parton energy loss becomes relatively more important, until the smooth vanishing of all nuclear effects at the highest energies. The model finally presents problems describing the correct A and z dependencies of the transverse momentum broadening. This issue definitely requires further investigations on both the experimental and theoretical front to be resolved.

VI. ACKNOWLEDGEMENTS

We acknowledge many fruitful discussions with A. Accardi, F. Arleo, and S. Peigne. This work has received funding from the European Research Council (ERC) under the European

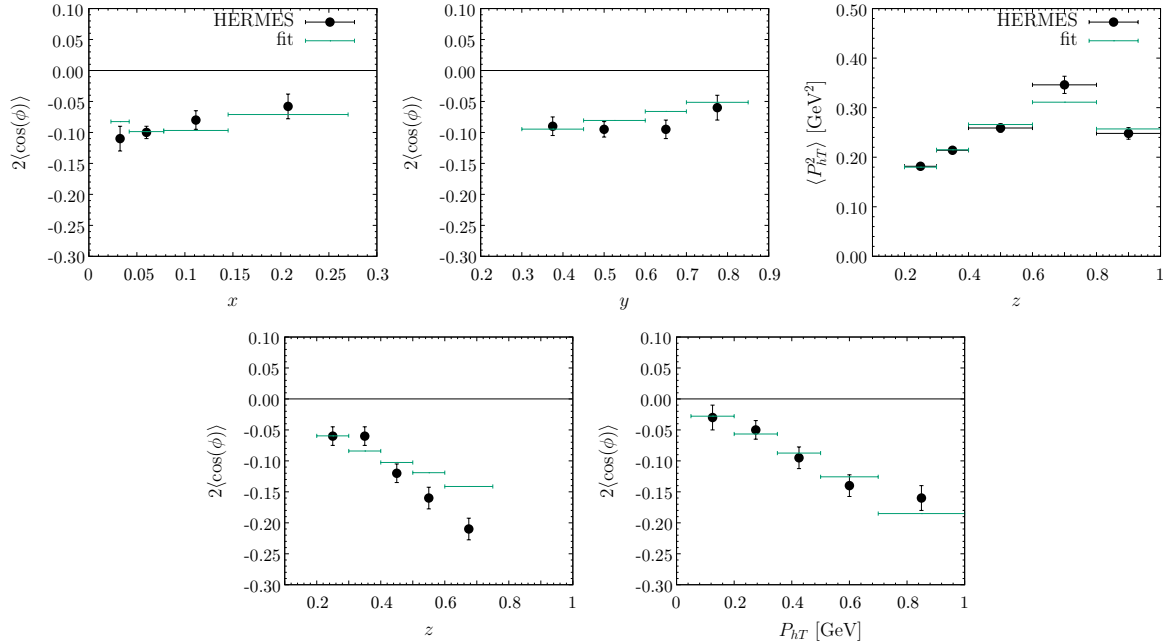


Figure 9: Predictions based on best fit results compared to the $\cos(\phi)$ asymmetry [39] and the hadronic widths [40] measured in π^+ electroproduction on a proton target at HERMES.

Union’s Horizon 2020 research and innovation programme (Grant agreement No. 804480)

Appendix A: Hadronic widths

Numerous extraction of parameters characterizing transverse momentum spectra within TMD phenomenology are available in the literature. In the present work, however, we wish to provide a dedicated extraction within the specific theoretical framework adopted and tailored to the analysis of the nuclear dataset. For that purpose, we present in the right panel of Fig. (9) the hadronic width as a function of z . On the other hand, the width parametrization in Eq. (7) shows a quadratic behaviour as a function of z , at variance with the data which shows a dampening at large z . To accommodate this behavior within the structure of Eq. (7) and considering the findings of Ref.[28,29], we assume a fragmenting width of the type $\langle p_{\perp}^2 \rangle = (A + Bz^2)(1 - z)^C$ and a constant, z -independent, distribution width $\langle k_{\perp}^2 \rangle = D$. The four-parameter functional form is then given by

$$\langle P_{hT}^2 \rangle = (A + Bz^2)(1 - z)^C + z^2 D. \quad (\text{A1})$$

A	B	C	D
$0.15 \pm 0.01 \text{ GeV}^2$	$1.08 \pm 0.15 \text{ GeV}^2$	0.69 ± 0.07	$0.052 \pm 0.002 \text{ GeV}^2$

Table III: Parameters controlling the hadronic widths on a proton target obtained from the fit of HERMES data.

In such a form, however, the D parameter can not be precisely determined by fits to hadronic spectra alone. We therefore reconsider the cross section in Eq. (2). There, the structure function proportional to $\cos \phi$, the so-called Cahn contribution, can be written, under the approximation used in this paper, as

$$F_{UU}^{\cos \phi_h} = -2x_B \frac{P_{hT}}{Q} \sum_q e_q^2 f_{q/P}(x_B, Q^2) D_{h/q}(z, Q^2) \frac{z \langle k_{\perp}^2 \rangle}{\langle P_{hT}^2 \rangle} \frac{e^{-P_{hT}^2 / \langle P_{hT}^2 \rangle}}{\pi \langle P_{hT}^2 \rangle}. \quad (\text{A2})$$

in whose terms one can then define the following asymmetry

$$2\langle \cos \phi \rangle = 2 \frac{\int d\phi d\sigma \cos \phi}{\int d\phi d\sigma} = \frac{2(2-y)\sqrt{1-y} F_{UU}^{\cos \phi}}{[1+(1-y)^2] F_{UU}}. \quad (\text{A3})$$

The latter does not contain additional unknowns with respect to F_{UU} and, important for our purpose, is proportional to $\langle k_{\perp}^2 \rangle$: its inclusion in the fit allows us to constrain the parameter D , which would be otherwise under-unconstrained. The parameters are then obtained by a minimization procedure performed with the help of the MINUIT package [41]. We include in the fit the widths extracted by Gaussian fits of π^+ transverse momentum spectra off a proton target and the corresponding $\cos(\phi)$ asymmetry, both published by the HERMES Collaboration [39, 40]. We assume that the asymmetry is saturated by the Cahn effect, and the Boer–Mulders contribution is negligible. The best-fit results are compared to data in Fig. (9) and the corresponding parameters are reported in Tab. (III). The fit returns a χ^2 per *d.o.f.* of around 2, and its large value is traced back to the discrepancy observed in the description of the asymmetry as a function of z . Despite this, the obtained parametrization gives a good representation of $\langle P_{hT}^2 \rangle$, as shown in the right panel of Fig. (9), and therefore is used as a default choice in all our simulations.

[1] R. L. Workman et al. (Particle Data Group), “Fragmentation Functions in e^+e^- , ep , and pp Collisions,” in Prog. Theor. Exp. Phys. **2022**, 083C01 (2022) Chap. 19, p. 375.

- [2] A. Accardi, F. Arleo, W. K. Brooks, D. D'Enterria, and V. Muccifora, Riv. Nuovo Cim. **32**, 439 (2010), arXiv:0907.3534 [nucl-th] .
- [3] H. Avakian, A. Bressan, and M. Contalbrigo, Eur. Phys. J. A **52**, 150 (2016), [Erratum: Eur.Phys.J.A 52, 165 (2016)].
- [4] A. Bacchetta, Eur. Phys. J. A **52**, 163 (2016), arXiv:2107.06772 [hep-ph] .
- [5] M. Alrashed, D. Anderle, Z.-B. Kang, J. Terry, and H. Xing, Phys. Rev. Lett. **129**, 242001 (2022), arXiv:2107.12401 [hep-ph] .
- [6] J. Ashman et al. (European Muon Collaboration), Z. Phys. C **52**, 1 (1991).
- [7] A. Airapetian et al. (HERMES Collaboration), Nucl.Phys. **B780**, 1 (2007), arXiv:0704.3270 [hep-ex] .
- [8] A. Airapetian et al. (HERMES), Phys. Lett. B **684**, 114 (2010), arXiv:0906.2478 [hep-ex] .
- [9] A. Airapetian et al. (HERMES), Eur. Phys. J. A **47**, 113 (2011), arXiv:1107.3496 [hep-ex] .
- [10] S. Moran et al. (CLAS), Phys. Rev. C **105**, 015201 (2022), arXiv:2109.09951 [nucl-ex] .
- [11] B. Kopeliovich, J. Nemchik, E. Predazzi, and A. Hayashigaki, Nucl.Phys. **A740**, 211 (2004), arXiv:hep-ph/0311220 [hep-ph] .
- [12] A. Accardi, V. Muccifora, and H.-J. Pirner, Nucl.Phys. **A720**, 131 (2003), arXiv:nucl-th/0211011 [nucl-th] .
- [13] A. Accardi, D. Grunewald, V. Muccifora, and H. J. Pirner, Nucl. Phys. A **761**, 67 (2005), arXiv:hep-ph/0502072 .
- [14] B. Guiot and B. Z. Kopeliovich, Phys. Rev. C **102**, 045201 (2020), arXiv:2001.00974 [hep-ph] .
- [15] F. Arleo, Eur. Phys. J. C **30**, 213 (2003), arXiv:hep-ph/0306235 .
- [16] S. Domdey, D. Grunewald, B. Kopeliovich, and H. Pirner, Nucl.Phys. **A825**, 200 (2009), arXiv:0812.2838 [hep-ph] .
- [17] J.-H. Gao, Z.-T. Liang, and X.-N. Wang, Phys. Rev. C **81**, 065211 (2010), arXiv:1001.3146 [hep-ph] .
- [18] L.-H. Song and C.-G. Duan, Phys.Rev. **C81**, 035207 (2010).
- [19] Y.-K. Song, J.-H. Gao, Z.-T. Liang, and X.-N. Wang, Phys. Rev. D **89**, 014005 (2014), arXiv:1308.1159 [hep-ph] .
- [20] Y.-K. Song, Z.-T. Liang, and X.-N. Wang, Phys. Rev. D **89**, 117501 (2014), arXiv:1402.3042 [nucl-th] .

- [21] P. Ru, Z.-B. Kang, E. Wang, H. Xing, and B.-W. Zhang, *Phys. Rev. D* **103**, L031901 (2021), arXiv:1907.11808 [hep-ph] .
- [22] W. K. Brooks and J. A. López, *Phys. Lett. B* **816**, 136171 (2021), arXiv:2004.07236 [hep-ph] .
- [23] K. Gallmeister and U. Mosel, *Nucl. Phys. A* **801**, 68 (2008), arXiv:nucl-th/0701064 .
- [24] W. Ke, Y.-Y. Zhang, H. Xing, and X.-N. Wang, (2023), arXiv:2304.10779 [hep-ph] .
- [25] A. Bacchetta, U. D’Alesio, M. Diehl, and C. A. Miller, *Phys. Rev. D* **70**, 117504 (2004), arXiv:hep-ph/0410050 .
- [26] A. Bacchetta, M. Diehl, K. Goeke, A. Metz, P. J. Mulders, and M. Schlegel, *JHEP* **02**, 093 (2007), arXiv:hep-ph/0611265 .
- [27] B. Kopeliovich, J. Nemchik, and I. Schmidt, *Nucl.Phys.* **A782**, 224 (2007), arXiv:hep-ph/0608044 [hep-ph] .
- [28] N. Armesto et al., *Phys. Rev. C* **86**, 064904 (2012), arXiv:1106.1106 [hep-ph] .
- [29] F. Arleo, *JHEP* **11**, 044 (2002), arXiv:hep-ph/0210104 .
- [30] R. Baier, Y. L. Dokshitzer, A. H. Mueller, S. Peigne, and D. Schiff, *Nucl. Phys. B* **483**, 291 (1997), arXiv:hep-ph/9607355 .
- [31] R. Baier, Y. L. Dokshitzer, A. H. Mueller, and D. Schiff, *JHEP* **0109**, 033 (2001), arXiv:hep-ph/0106347 [hep-ph] .
- [32] X.-N. Wang, Z. Huang, and I. Sarcevic, *Phys. Rev. Lett.* **77**, 231 (1996), arXiv:hep-ph/9605213 .
- [33] R. Baier, Y. L. Dokshitzer, A. H. Mueller, S. Peigne, and D. Schiff, *Nucl. Phys. B* **484**, 265 (1997), arXiv:hep-ph/9608322 .
- [34] R. Baier, Y. L. Dokshitzer, A. H. Mueller, and D. Schiff, *Nucl.Phys.* **B531**, 403 (1998), arXiv:hep-ph/9804212 [hep-ph] .
- [35] C. Ciofi degli Atti and S. Simula, *Phys. Rev. C* **53**, 1689 (1996), arXiv:nucl-th/9507024 .
- [36] K. Kovarik et al., *Phys. Rev. D* **93**, 085037 (2016), arXiv:1509.00792 [hep-ph] .
- [37] D. de Florian, R. Sassot, M. Epele, R. J. Hernández-Pinto, and M. Stratmann, *Phys. Rev. D* **91**, 014035 (2015), arXiv:1410.6027 [hep-ph] .
- [38] M. Boggione, M. Diefenthaler, S. Dolan, L. Gamberg, W. Melnitchouk, D. Pitonyak, A. Prokudin, N. Sato, and Z. Scalyer (Jefferson Lab Angular Momentum (JAM)), *JHEP* **04**, 084 (2022), arXiv:2201.12197 [hep-ph] .

- [39] A. Airapetian et al. (HERMES), Phys. Rev. D **87**, 012010 (2013), arXiv:1204.4161 [hep-ex] .
- [40] A. Airapetian et al. (HERMES), Phys. Rev. D **87**, 074029 (2013), arXiv:1212.5407 [hep-ex] .
- [41] F. James and M. Roos, Comput. Phys. Commun. **10**, 343 (1975).